Quaternary Research 80 (2013) 562–574

Contents lists available at ScienceDirect

Quaternary Research

journal homepage: www.elsevier.com/locate/yqres

Climate archives from 90 to 250 ka in horizontal and vertical ice cores from the Allan Hills Blue Ice Area, Antarctica

Nicole E. Spaulding [a,*], John A. Higgins [b], Andrei V. Kurbatov [a], Michael L. Bender [b], Steven A. Arcone [c], Seth Campbell [a,c], Nelia W. Dunbar [d], Laura M. Chimiak [b], Douglas S. Introne [a], Paul A. Mayewski [a]

[a] Climate Change Institute, School of Earth and Climate Sciences, University of Maine, Orono, ME, USA
[b] Department of Geosciences, Princeton University, Princeton, NJ, USA
[c] US Army Cold Regions Research and Engineering Laboratory, Hanover, NH, USA
[d] Earth and Environmental Science Department New Mexico Tech, Socorro, NM, USA

ARTICLE INFO

Article history:
Received 7 January 2013
Available online 3 October 2013

Keywords:
Marine Oxygen Isotope Stage 5.5
Marine Oxygen Isotope Stage 7
Termination II
Termination III
Blue ice area
Allan Hills
δD
$^{40}Ar_{atm}$
$\delta^{18}O_{atm}$
Ice core

ABSTRACT

Terrestrial meteorite ages indicate that some ice at the Allan Hills blue ice area (AH BIA) may be as old as 2.2 Ma. As such, ice from the AH BIA could potentially be used to extend the ice core record of paleoclimate beyond 800 ka. We collected samples from 5 to 10 cm depth along a 5 km transect through the main icefield and drilled a 225 m ice core (S27) at the midpoint of the transect to develop the climate archive of the AH BIA. Stable water isotope measurements (δD) of the surface chips and of ice core S27 yield comparable signals, indicating that the climate record has not been significantly altered in the surface ice. Measurements of $^{40}Ar_{atm}$ and $\delta^{18}O_{atm}$ taken from ice core S27 and eight additional shallow ice cores constrain the age of the ice to approximately 90–250 ka. Our findings provide a framework around which future investigations of potentially older ice in the AH BIA could be based.

Introduction

A global array of climate proxies, including ice cores, marine sediment cores (e.g. Shackelton and Opdyke, 1976; Lisiecki and Raymo, 2005), and speleothems (e.g. Winograd et al., 1992) have provided major breakthroughs in our understanding of the driving mechanisms of past climate change. Unlike other materials, ice cores contain trapped gases, which can be used to reconstruct paleoatmospheric composition. As a result of this advantage, ice cores have enabled some of the most fundamental discoveries in climate science. For example, the identification of abrupt high-magnitude changes in climate (Dansgaard et al., 1993; Grootes et al., 1993; Mayewski et al., 1994) and the close association between atmospheric greenhouse gases and Antarctic temperature (EPICA, 2004) can be attributed to the study of ice cores. Additionally, within ice cores, it is possible to sub-annually resolve some proxies including concentrations of soluble compounds and insoluble particle chemistry. However, traditional ice coring activities are limited by the deepest practical drilling depth and the availability of old ice. Blue ice areas offer a complementary approach that removes these limitations. In this paper we investigate the age of blue ice in the Allan Hills area of East Antarctica and show that it may contain climatic information relevant to the behavior of the Ross Ice Shelf and perhaps the West Antarctic Ice Sheet under warmer climate scenarios (Raymo and Mitrovica, 2012).

While ice cores form an essential climate archive, their use is not without challenges. Their primary restriction is latitudinal, with most long ice cores being collected in the polar regions. Even within Antarctica the number of places an undisturbed long record of climate containing well-preserved ice chemistry and atmospheric gas signals can be collected is limited (Severinghaus et al., 2010). This is problematic, as it has been demonstrated that significant regional variability exists in the ice-core record of changes in temperature, atmospheric circulation, wind intensity, and sea-ice coverage among other climate parameters (e.g. Dixon et al., 2011) and we must obtain old ice from multiple locations to confirm significant findings. There are at present, six high-resolution ice-core temperature records (Vostok, EPICA Dome C, EPICA Dronning Maud Land, Dome Fuji, Taylor Dome, and TALDICE) that fully encompass the present to the penultimate glacial maximum (Petit et al., 1999; Steig et al., 2000; Grootes et al., 2001; EPICA Community Members, 2006; Jouzel et al., 2007; Kawamura et al., 2007; Masson-Delmotte et al., 2011; Stenni et al., 2011). Of those six records only four extend beyond the penultimate glacial maximum. Additionally, the locations from

* Corresponding author. Fax: +1 207 581 1203.
E-mail address: nicole.spaulding@maine.edu (N.E. Spaulding).

0033-5894/$ – see front matter © 2013 University of Washington. Published by Elsevier Inc. All rights reserved.
http://dx.doi.org/10.1016/j.yqres.2013.07.004

which long ice cores can be collected are generally sites of very low accumulation. The low initial annual layer thickness can result in irresolvable or missing layers at depth. As a result of these limitations, exploring potentially complementary ice archives in unconventional locations, such as blue-ice areas (BIAs), is a goal to be pursued.

Paleoclimate records from several Antarctic BIAs have been developed over the last decade. Each of these records was collected in coastal or mountainous regions where traditional deep ice cores could not be drilled and at significantly lower resource investment. Each BIA record was also able to provide higher temporal resolution than usual in deep ice cores. The records from Scharffenbergbotnen (Sinisalo et al., 2007), South Yamato (Nakawo et al., 1988; Machida et al., 1996; Moore et al., 2006) and Mt. Moulton (Custer, 2006; Popp, 2008; Korotkikh et al., 2011) demonstrate that paleoclimate reconstructions from BIAs can be used to augment the already detailed ice-core record of past climate change, if robust age determination techniques are employed.

The primary objectives of this paper are to determine the age of ice within the main icefield (MIF) of the Allan Hills blue-ice area (AH BIA) and evaluate its surface-ice climate record. We use measurements of $^{40}Ar_{atm}$, $\delta^{18}O_{atm}$ and δD from a series of ice cores to constrain the age and paired δD records to assess the quality of the climate record at the ice surface.

Glaciological and regional setting

The AH BIA is located near the northwest corner of the McMurdo Dry Valleys in South Victoria Land, East Antarctica (Fig. 1). Ice flowing into the AH BIA at the present time has an accumulation area located only ~20 km upstream (Faure et al., 1992), as such it is ideally located to capture climatic changes within the Ross Embayment and the Transantarctic Mountains. This is particularly true of paleotemperature signals because the majority of precipitation reaching the accumulation area of the AH BIA must first cross the Ross Ice Sheet (King and Turner, 1997; Sinclair et al., 2010).

As in most BIAs, ice flow through and within the MIF of the AH BIA is controlled by complex sub-ice topography and the presence of outcropping nunataks. Bedrock conditions within the AH BIA are detailed in Fudali (1982, 1989), Faure and Buchanan (1987), and Delisle and Sievers (1991); ice flow measurements are discussed in Schultz et al. (1990) and Spaulding et al. (2012). Briefly, ice enters the MIF from the south/southwest with a horizontal velocity of 50 cm a^{-1} and then follows the north/northeasterly path shown as a pink swath in Figure 1. Spaulding et al. (2012) used high-precision GPS measurement to determine that path and individual velocity vectors can be seen in Figure 2 of their publication. Horizontal ice velocities decrease to a nearly stagnant 1.5 cm a^{-1} near the base of the Allan Hills nunatak. Between these points, where satellite imagery indicates bare ice, positive vertical velocities of 1–3 cm a^{-1} and ablation rates (~2 cm a^{-1}) in excess of the accumulation rates in the surrounding snow plains are reported (Spaulding et al., 2012). The low horizontal velocities, emergent vertical velocities and net ice loss through ablation combine to bring older ice to the surface and maintain its exposure over long periods of time. For a more in-depth discussion of ice dynamics in blue-ice areas, please refer to Nagata (1978), Whillans and Cassidy (1983), or Bintanja (1999). As ice flows through the MIF, small-scale compression and extension forces reshape the appearance of the present-day surface, creating the cracking, ridging, and sharp changes in surface slope (Fig. 2) observed in many locations during our first field season. The continuity of ash layers crossing transect A–B (Fig. 1) suggests that these forces have not caused significant reordering or offsetting of the original stratigraphy (Dunbar et al., 1995).

Determining the age of ice exposed within BIAs is particularly challenging. Traditionally, ice-flow models are used to provide a first approximation of the age of ice at the surface and at depth. The required input for such models includes accumulation rates, high-resolution bedrock topography, and horizontal velocities. At the AH BIA, high-

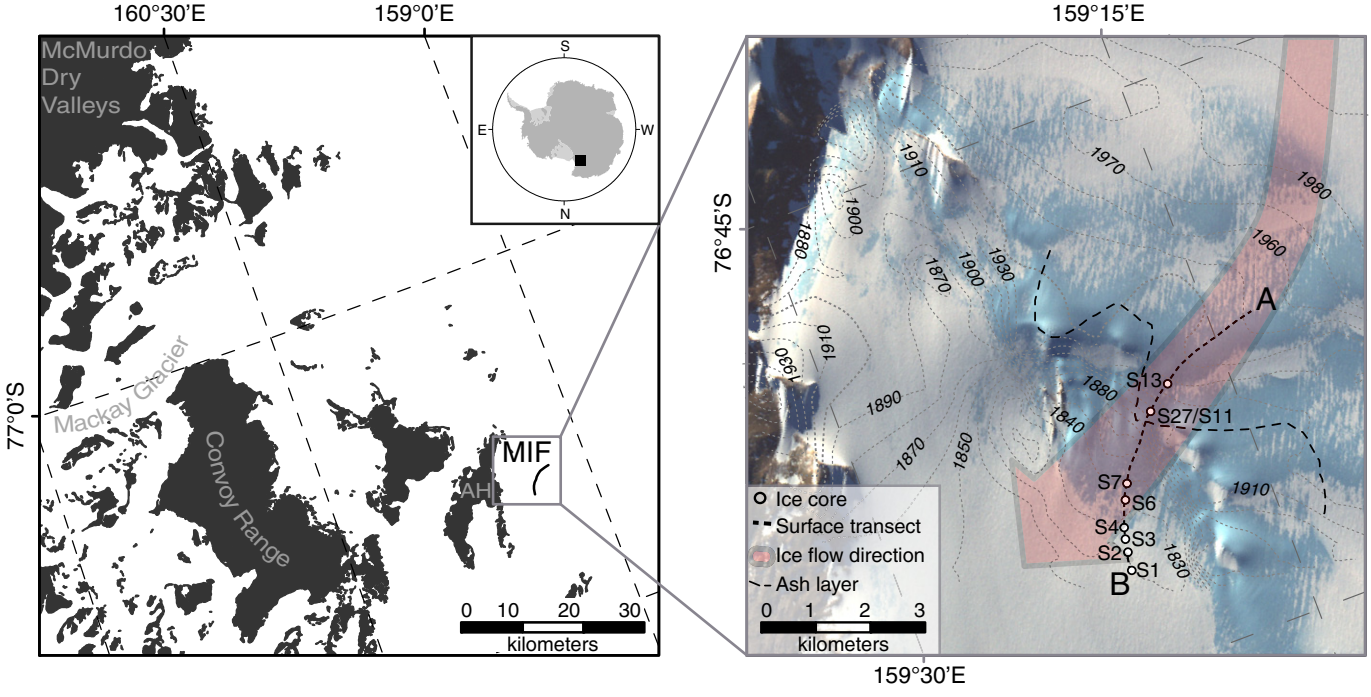

Figure 1. Eight shallow ice cores, one 225 m core (S27) and 536 surface samples were collected from the main icefield (MIF) of Allan Hills blue ice area during field seasons in 2010 and 2011. The surface samples were collected at 10 m intervals along transect A–B for stable water isotope analysis. Transect A–B is largely within the flow zone described in Spaulding et al., 2012. Only one of the many ash layers (Dunbar et al., 1995) crossing transect A–B was used as a stratigraphic control point.

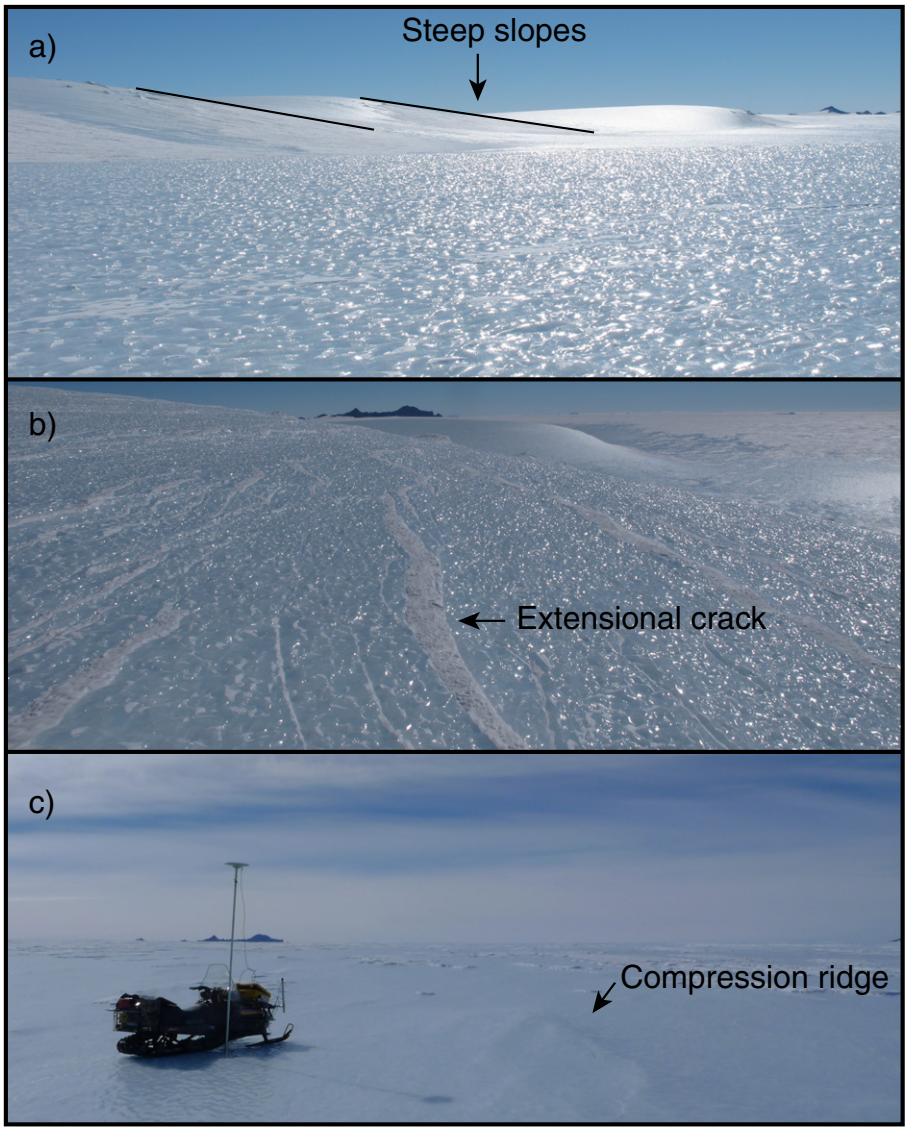

Figure 2. The interaction of ice flow with bedrock topography, high rates of ablation, sharp seasonal temperature changes, and redeposition of blowing snow create unequal and very dynamic surface conditions. We observed (a) relatively steep surface slopes, (b) extensional cracking and (c) small-scale compression ridging at a number of locations along transect A–B. They do not appear to have impacted the continuity of the climate record along transect A–B.

resolution (<100 m) bedrock data are not available and modern accumulation rates are poorly constrained. Additionally, the horizontal and vertical flow of ice has the potential to distort (relative to predictions from simplified flow models) the duration of climate events identified within the surface ice and cause overall thinning of the ice column. In the absence of a flow model, the terrestrial ages of meteorites collected at the ice surface have been used to estimate the age of the ice. Because meteorites may remain exposed at the surface of an ice sheet long after the ice that originally encased them has ablated away, the terrestrial age of a meteorite (a measure of the time elapsed since it entered the earth's atmosphere) represents an upper age limit for the surrounding ice. Several teams of researchers have collected meteorites in the Allan Hills (Cassidy et al., 1977, 1992 and references therein; Harvey, 2003 and references therein) and hundreds of these meteorites have been dated (Nishiizumi, 2006; Nishiizumi and Welten, 2008). The majority of meteorite terrestrial ages for the AH BIA are between 100 and 400 ka (Nishiizumi et al., 1989); however a continuous range of ages up to 1 Ma and a single 2.2 Ma specimen have also been reported (Scherer et al., 1997). The continuous sequence of meteorite terrestrial ages, the lack of evidence for offsetting of layers and the low surface ice velocity indicate that the AH BIA is an ideal location for the collection of horizontal trenches and ice cores to be used for paleoclimate reconstruction.

Materials and methods

Sampling strategy

Our surface sampling strategy was designed to ensure that glacial/interglacial changes in δD of the surface ice (<10 cm below the ice–air interface) would be adequately captured. We sampled at 10 m intervals along an ~5 km North–South transect through the MIF (Fig. 1, labeled A–B) based on the hypothesis that the ages of actively ablating ice within the MIF, like those of the meteorites, were continuous between 0 and 1 Ma and that each of these ages could be sampled. Transect A–B is within the zone suggested by Spaulding et al. (2012) as likely to be continuous. The 10 m spacing ensured that each sample was separated by a no more than 2 ka (1 Ma/5500 m = 0.2 ka/m), which would

provide at least five points per interglacial period (assuming a duration of 10–16 ka; Tzedakis et al., 2012). Using the spacing outlined above, we collected 536 surface samples (~50 g each) 5–10 cm below the ice. We chose to collect samples from bare ice patches up to 20 m away from the profile line to avoid locations where thick crusts of windblown snow (>30 cm) had accumulated along the transect.

Ice cores collected during the first field season were to be used to establish ice ages along transect A–B. Our ice coring strategy was designed to ensure that an adequate volume of ice was collected along what was presumed to be the most valuable (oldest) section of transect A–B, but also provide coverage of the younger portion. The first four cores (S1–S4) were collected in the accumulation zone nearest to the nunatak and were separated by ~0.25 km. The next two cores (S6, S7) were collected beginning ~0.5 km away from the fourth, within the ablation zone. The steep slope encountered along transect A–B dictated the location of the final two cores (S11, S13). Each of the eight cores was drilled to approximately 15 m.

The following season our aim was to collect an ice core that could be used to verify that differential ablation, stratigraphic deformation and/or flow mixing had not impacted the continuity or integrity of the signal observed in the surface ice samples and to provide additional ice for trapped gas measurements. A 225 m core (S27) was drilled at approximately the mid-point of transect A–B (near S11) using an ECLIPSE electromechanical ice drill. At this site the ice thickness was close to its minimum along transect A–B, as identified using ground penetrating radar (Fig. 3 — 76.70°S, 159.31°E). S27 was expected to contain the same sequence of ice exposed in the 2.67 km of transect downflow. We aimed to recover the oldest ice along transect A–B, which may be present frozen to bedrock, but were only able to drill to 225 m depth (70% of the estimated column thickness) during a single field season.

Analytical methods

Stable water isotopes

The stable water isotope samples from ice core S27 and the surface ice were used as a proxy for regional paleotemperatures (e.g. Dansgaard et al., 1973; Jouzel et al., 1997). To produce samples from S27, a 2.5 cm thick slab of ice was cut (parallel to the vertical axis) from the outside of each 1 m section of ice core. These slabs were sub-sampled at 15 cm resolution in a −20°C working freezer at the Climate Change Institute. Because some portions of the core were heavily fractured continuous sections were not available at all depths. Each sub-sample was melted in a sealed plastic bag at room temperature, vigorously shaken, then decanted into an 18 ml plastic scintillation vial. In order to prevent fractionation, all vials were refrozen and stored below −10°C until the time of analysis. The samples were analyzed in 2011 for δD by continuous flow isotope mass spectrometry, via Cr pyrolysis at 1050°C with an Eurovector elemental analyzer coupled to a Micromass Isoprime mass spectrometer (±0.05‰ precision). Each run contained 99 individual waters (89 samples and 10 standards), analyzed in triplicate over a 24-hour period. Measurement of instrument drift and daily calibration was accomplished by measuring at interval three calibrated in-house water standards: BBB (an average Maine freshwater from the Bear Brook watershed), ASS (Antarctic Surface Snow) and LAP (Light Antarctic Precipitation). These standards, which span a wide range of naturally occurring isotopic values, were calibrated against the internationally accepted water isotope standards: SMOW (Standard Mean Ocean Water), SLAP (Standard Light Antarctic Precipitation) and GISP (Greenland Ice Sheet Precipitation). Surface ice samples were processed at McMurdo Station's Crary Laboratory using the same melting and decanting procedure as above. As an extra precaution against evaporation during shipment, the scintillation vials were sealed with both paraffin wax and electric tape. The sealed samples were refrozen and shipped to the University of Maine where they remained frozen (below −10°C) until the time of analysis. Each sample was analyzed in 2010 for $\delta^{18}O$ via equilibration with CO_2 gas at 25°C (e.g. Craig, 1961). Equilibrated gas was admitted from a Micromass Multiprep peripheral to a VG SIRA dual inlet mass spectrometer for measurement (±0.5‰ precision). Sixty individual waters were analyzed during each run, with every fifth sample measured being an in-house laboratory standard as described above (12 standards, 48 samples). Surface $\delta^{18}O$ values were converted to δD value via a local meteoric water curve developed from samples where both δD and $\delta^{18}O$ were intentionally measured (see Fig. 4b and Supplementary Table 1).

Trapped-gas measurements. Each shallow core site was sampled for the isotopic composition of trapped gases ($^{40}Ar_{atm}$, $\delta^{18}O$ of atmospheric O_2, and $\delta^{15}N$ of atmospheric N_2) between 11.9 and 18.7 m. With the exception of S2, the top 12 m of each ice core was not sampled, as previous work in blue ice areas (T. Sowers, personal communication) suggests that gas composition at these depths may be altered by cracks and fracturing. High-resolution samples between 2 and 15 m depth

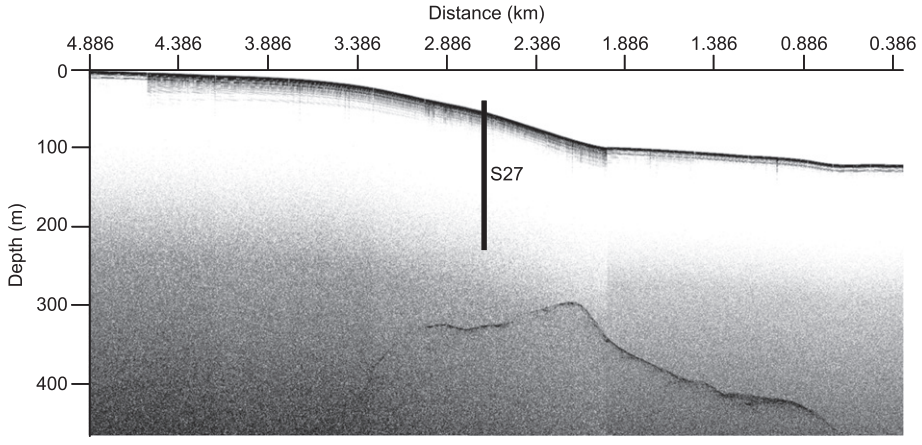

Figure 3. Ground penetrating radar (GPR) data collected along transect A–B was used to guide the selection of a drill site with minimum ice thickness and stratigraphic disturbances. A 225 m core (S27) was drilled just upslope of the 300 m ice thickness minima where surface slopes were suitable for drilling. The radar survey was conducted using Geophysical Survey Systems, Inc. (GSSI) SIR-3000 16-bit control unit coupled with a model 3107 (100 MHz) transceiver monostatic antenna and assuming a dielectric constant of 3.15 and a time range of either 6000 or 4567 ns. The RADAN data processing software was used to distance normalize 15 individual profiles along A–B, which were then merged and surface normalized as a single unit.

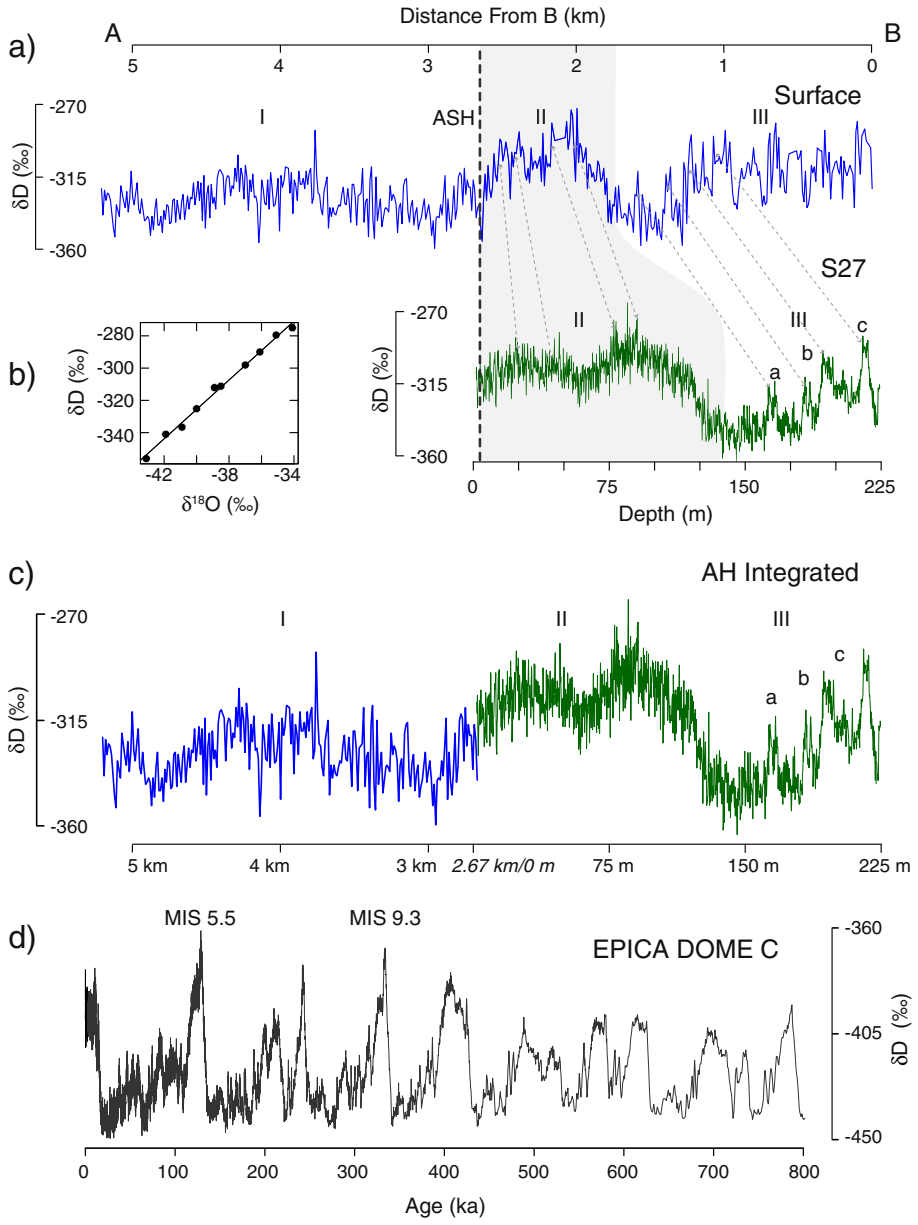

Figure 4. a) The δD profile along transect A–B contains three recognizable intervals (I–III) rising 50–90‰ above the ~360‰ baseline value. The magnitude of these intervals, which we term as "Events" throughout the manuscript, are similar in scale to the transitions interpreted to be glacial/interglacial changes in deep ice cores. Ice core S27 contains Event II and a more clearly defined Event III. The surface ice and S27 were correlated using the tie-points shown and those listed in Table 4. Note that the final ice core depth is matched to 860 m at the surface. b) For comparisons, a local meteoric water line was used to convert the measured $\delta^{18}O$ of surface samples to δD. c) The two records were spliced at their point of intersection to maximize temporal coverage and sampling resolution. This is the AH integrated δD record.

from S2 were measured for trapped gases to test for potential contamination of near-surface gas records. Three samples for $\delta^{40/38}Ar$ and $\delta^{38/36}Ar$ measurements were taken from depths ranging from 109 to 215 m within ice core S27. Samples were also taken approximately every 4 m along the entire cored range of S27 for trapped gases ($\delta^{18}O$ of atmospheric O_2 and $\delta^{15}N$ of atmospheric N_2).

Analytical protocols for measurements $\delta^{40/38}Ar$, $\delta^{38/36}Ar$ and $\delta^{18}O$ of trapped gases are modified after Bender et al. (2008) and Dreyfus et al. (2007), respectively, and are briefly reviewed here. Precise measurements of $\delta^{40/38}Ar$ and $\delta^{38/36}Ar$ required 550–650 g of ice, cut from a continuous length of 3″ diameter core, with the outer 2–3 mm of each surface removed prior to melting. To extract and purify Ar from trapped air, we placed the ice samples in glass flasks sealed with Viton O-rings, cooled the flasks to −40°C, and pumped to vacuum. We melted the ice, equilibrated water and headspace, and drained the water as described by Emerson et al. (1995). Ar was then purified from residual water, CO_2, O_2 and N_2 on a vacuum line using a liquid N_2 trap and a SAES ST 101 Getter heated to 900°C and transferred to a ~12 scc stainless steel sample tube submerged in liquid He for Ar isotopic analysis. $\delta^{40/38}Ar$ and $\delta^{38/36}Ar$ were measured at Princeton University on a Finnigan MAT 252 isotope ratio mass spectrometer with collectors configured for the simultaneous measurement of masses 36, 38, and 40. A customized inlet was used to maximize sensitivity for relatively small Ar samples (see Bender et al., 2008 for details). $\delta^{40/38}Ar$ and $\delta^{38/36}Ar$ values are used to calculate $^{40}Ar_{atm}$ ages ($\delta^{40/38}Ar - 1.002 * \delta^{38/36}Ar$), which reflect the slow accumulation of ^{40}Ar in the atmosphere over geologic time. Using multiple isotopes in the calculation removes the effects of mass-dependent fractionation associated with sample

Table 1
Measurements of $^{40}Ar_{atm}$ in Vostok and Allan Hills ice cores. Uncertainties in $^{40}Ar_{atm}$ reflect analytical uncertainties from the mass spectrometer. Reported ages group samples from each site, with the associated uncertainty reflecting the spread of ages for that site. Although variations in age with depth may exist, most samples are taken from a relatively narrow depth interval (<10 m) and we assume on this scale that we are sampling ice of approximately the same age. Expected down-core variations at site S27 are likely too small to be resolved by our measurements.

Sample	Depth (m)	$\delta^{15}N$ (‰)	1σ	$\delta^{18}O_{atm}$ (‰)	1σ	$\delta O_2/N_2$ (‰)	1σ	$\delta Ar/N_2$ (‰)	1σ
PU air		0	0.013	0	0.035	0	1.20	0	0.77
Site 2	2.10	0.061		0.139		1.71		−6.74	
Site 2	2.65	0.052	0.034	0.323	0.067	−1.98	2.83	−5.27	1.51
Site 2	3.10	0.057	0.022	0.183	0.058	7.85	5.13	−0.49	3.18
Site 2	3.50	0.067	0.071	0.309	0.099	−0.43	7.00	−7.27	3.31
Site 2	4.10	0.065	0.013	0.276	0.049	7.64	2.39	−1.45	4.55
Site 2	5.50	0.066	0.057	0.184	0.051	12.77	10.08	3.02	3.05
Site 2	6.00	0.110	0.009	0.329	0.068	2.76	1.98	−0.93	3.94
Site 2	7.80	0.075	0.015	0.529	0.042	−8.94	2.26	−9.80	2.72
Site 2	8.67	0.099	0.030	0.408	0.021	−5.77	1.28	−1.77	4.07
Site 2	9.50	0.105		0.378		−16.36		−12.17	
Site 2	10.20	0.116	0.030	0.286	0.052	−2.84	2.94	−3.21	0.94
Site 2	10.80	0.081		0.366		−11.21		−6.75	
Site 2	11.70	0.072	0.042	0.346	0.073	−7.65	2.03	−4.14	1.32
Site 2	12.40	0.114	0.026	0.320	0.030	−3.05	2.91	−2.75	2.80
Site 2	12.95	0.022	0.010	0.397	0.048	−1.39	1.40	−3.88	4.80
Site 2	13.20	0.071	0.026	0.439	0.065	9.35	4.34	5.51	1.90
Site 2	14.40	0.097		0.478		−12.20		−8.84	
Site 2	15.20	0.065		0.297		−8.19		−0.77	
Site 1	15.00	0.125	0.010	1.071	0.047	−1.30	3.19	−1.62	1.17
Site 3	14.60	0.090	0.014	0.261	0.074	−7.75	5.12	−4.34	3.95
Site 4	15.10	0.153	0.067	0.018	0.004	−3.91	2.21	−5.89	2.35
Site 6	12.40	0.151	0.011	−0.015	0.056	−2.18	5.71	−0.91	3.38
Site 7	14.30	0.132	0.002	0.672	0.017	−5.0	3.09	−3.4	2.82
Site 11	14.50	0.110	0.013	0.525	0.065	−16.40	3.21	−6.77	1.97
Site 13	17.80	0.179	0.020	−0.118	0.010	−4.84	1.67	−0.51	1.24

processing or gravitational settling within the firn (Schwander et al., 1988). Replicate measurements of Princeton air and contemporary (Holocene) samples from the Vostok ice core yielded indistinguishable $^{40}Ar_{atm}$ ages, with standard deviations of $^{40}Ar_{atm}$ of 0.016‰ (N = 55) and 0.010‰ (N = 5), respectively. Ar isotope measurements for ice from the AH BIA were normalized against Princeton air with negative values of $^{40}Ar_{atm}$ indicating the deficit in ^{40}Ar in the ancient atmosphere relative to modern.

The $\delta^{18}O$ of atmospheric O_2, $\delta^{15}N$ of N_2, $\delta Ar/N_2$, and $\delta O_2/N_2$, of trapped gases in AH BIA ice were measured on a Thermo Delta XP at Princeton University using 20–35 g of ice, prepped (cut and shaved) in a manner similar to $^{40}Ar_{atm}$ samples discussed above. Samples were then loaded into Ace-Thred bottles (~50 ml) with nylon bushings and 34 mm Viton o-ring and custom tops with 9 mm Louwers-Hapert valves and evacuated on the vacuum line in a −25°C water bath for 30 min. Once evacuated, samples were melted and equilibrated with the headspace on a rotator for ~3 h. Excess water was then drained and samples were transferred from the Ace sample vials to 15 scc stainless steel tubes submerged in liquid He. All samples are normalized to measurements of ~2 scc aliquots of Princeton air processed through the vacuum line. $\delta^{18}O_{atm}$, $\delta O_2/N_2$ and $\delta Ar/N_2$ are calculated from the measured $\delta^{18}O$ of O_2, $\delta O_2/N_2$, and $\delta Ar/N_2$ corrected for gravitational fractionation in the firn using the measured $\delta^{15}N$ of N_2. Replicate measurements of the Princeton air indicate a 1σ external reproducibility of 0.016‰, 0.046‰, 1.20‰, and 0.77‰ for $\delta^{15}N$ of N_2, $\delta^{18}O$ of O_2, $\delta O_2/N_2$, and $\delta Ar/N_2$, respectively.

Results

Stable water isotopes

The AH BIA surface δD record (Supplementary Table 2) has three distinct peaks, labeled I, II, and III in Figure 4a. These peaks will be referred to as Events I, II and III for the remainder of this manuscript. Each Event, by definition, rises by 50 to 90‰ above the minimum δD value. The magnitude of each Event is thus similar to the ~50‰ δD changes in the EDC ice core that have been interpreted as a change between glacial and interglacial climate modes (e.g. EPICA Community Members, 2006). Events I and III are more depleted by 29‰ and 9‰ (respectively) than the pronounced peak of Event II. Event III is characterized by a higher (less negative) average value (−310‰ vs −325‰) than Events II and I.

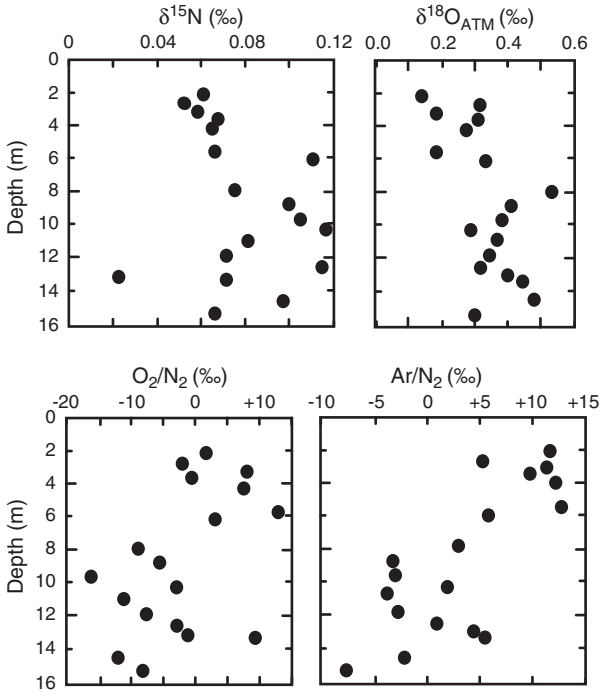

Figure 5. Depth profiles of $\delta^{18}O_{atm}$, $\delta^{15}N$ of N_2, $\delta O_2/N_2$, and $\delta Ar/N_2$ in the upper 15 m of ice core S2. We attribute variability in the chemistry of trapped gases in the upper 10 m to surface effects and contamination from modern/recent air.

Table 2
Measurements of $\delta^{15}N$ of N_2, $\delta^{18}O_{atm}$, $\delta O_2/N_2$, and $\delta Ar/N_2$ in shallow cores from the Allan Hills. Reported uncertainties reflect full sample replicates.

Sample	Lat/long	Depth (m)	$^{40}Ar_{atm}$ (‰)	1σ	Age (ka)	1σ
PU Air	40°20.922N/74°39.558′W		0	0.016	0	242
Vostok	72°12.002′S/106°47.999E	118.0	−0.002	0.021	−3	141
		124.5	0.001	0.018		
		180.0	0.014	0.014		
		180.3	−0.012	0.046		
		180.6	0.000	0.035		
Site 1	76°40.920′S/159°21.203E	12.5	−0.010	0.016	−121	386
		14.6	0.026	0.021		
Site 2	76°41.087′S/159°21.083E	4.4	−0.009	0.055	321	303
		7.0	−0.050	0.016		
		10.0	−0.027	0.023		
		13.5	−0.023	0.023		
		15.0	0.003	0.019		
Site 3	76°41.204′S/159°21.000E	12.0	−0.007	0.018	371	375
		15.0	−0.042	0.037		
Site 4	76°41.304′S/159°20.897E	12.5	−0.026	0.033	697	429
		15.0	−0.066	0.019		
Site 6	76°41.531′S/159°20.472E	17.0	−0.034	0.033	371	204
		17.3	−0.015	0.025		
Site 7	76°41.665′S/159°20.181E	14.3	−0.017	0.018	258	
Site 27	76°42.198′S/159°18.388E	109.6	−0.003	0.028	66	92
		189.0	−0.001	0.014		
		215.0	−0.011	0.032		
Site 11	76°42.198′S/159°18.388E	14.5	−0.002	0.016	235	375
		12.5	−0.033	0.009		
Site 13	76°42.377′S/159°17.376E	18.7	−0.014	0.017	212	
All sites			−0.018	0.021	269	315

The δD record from ice core S27 (Supplementary Table 3) has values ranging from −264‰ to −364‰ (average −316‰) and contains peaks that have magnitudes similar to Event II and III in the surface δD record. Ice core S27 was collected near the mid-point of transect A–B, therefore it is not expected to contain Event I, which occurs up flow from S27 in the youngest portion of the surface δD record. The magnitudes of Events II and III have the same proportionality as those observed in the surface record. The increased sampling resolution of S27 revealed greater detail in Event II and resolved three individual peaks (IIIa, IIIb, and IIIc — Fig. 4a) within Event III.

Shallow gas records from S2

High-resolution sampling from 2 to 15 m depth within S2 exhibits clear trends in the chemical composition of the upper ~10 m of ice (Table 1). The $\delta^{18}O$ of atmospheric O_2 declines towards the surface, consistent with some contamination from modern/recent air at very shallow depths (Fig. 5). Measured $\delta Ar/N_2$ and $\delta O_2/N_2$ values both increase towards the surface from more negative values at depth. Negative $\delta O_2/N_2$ and $\delta Ar/N_2$ are more typical of deep ice cores (Bender et al., 1995; Suwa and Bender, 2008) and the shift to more enriched values may reflect either preferential loss of N_2 or addition of O_2/Ar. Within deeper samples from S27, the effects of gas loss and/or exchange near the surface are minimized below 7 to 10 m depth, suggesting that drilling below 10 m depth is required to recover pristine gas records at the Allan Hills BIA.

$^{40}Ar_{atm}$ and $\delta^{18}O_{atm}$

$^{40}Ar_{atm}$ values and calculated ages are listed in Table 2. The average age for all 21 measurements is 269 ± 315 ka (1σ). This uncertainty is marginally larger than what we observe for replicate measurements of Princeton air or Holocene ice cores (1σ = 242 ka), suggesting that we are sampling ice of a relatively small range of ages. Measured $^{40}Ar_{atm}$ values do not show any statistically significant variability along the flow or with sampling depth, although we note that in general older ages are observed for S2–S6 compared to S7–S13, consistent with the exposure of progressively older ice towards the Allan Hills nunataks.

$\delta^{18}O_{atm}$ and $\delta^{15}N$ of N_2 values for both the shallow cores and S27 are listed in Tables 1 and 3, respectively. Although the spatial resolution afforded by the shallow cores is poor, measured $\delta^{18}O_{atm}$ values exhibit a range from +1.067‰ at S1 to −0.015‰ at S6, close to the range of ~1.5‰ observed for Pleistocene glacial cycles (Bender et al., 1994). The medium-resolution depth profile for $\delta^{18}O_{atm}$ at S27 shows coherent

Table 3
Measurements of $\delta^{15}N$ of N_2 and $\delta^{18}O_{atm}$ from S27. The similarity between $\delta^{18}O_{atm}$ measurements at the italicized depths and those in shallow cores of corresponding age (S11, S7 and S6) confirms the validity of the proposed depth/distance relationship.

Depth (m)	$\delta^{15}N$ (‰)	1σ	$\delta^{18}O_{atm}$ (‰)	1σ	Depth (mbis)	$\delta^{15}N$ (‰)	1σ	$\delta^{18}O_{atm}$ (‰)	1σ
7.06	*0.128*	*0.021*	*0.503*	*0.046*	*166.9*	*0.164*	*0.013*	*0.718*	*0.047*
13.89	0.105	0.007	0.673	0.040	171.11	0.129	0.023	0.237	0.030
18.37	0.125	0.001	0.571	0.018	172.09	0.106	0.001	0.047	0.035
28.20	0.127	0.036	0.487	0.056	176.97	0.125	0.011	−0.128	0.008
31.79	0.117	0.003	0.349	0.045	178.76	−0.111	0.331	0.067	0.023
37.17	0.115	0.014	0.202	0.039	181.47	0.113	0.008	−0.018	0.005
39.95	0.126	0.040	−0.014	0.021	187.58	0.111	0.001	0.195	0.078
46.94	0.126	0.009	−0.233	0.005	189.45	0.114	0.006	−0.017	0.034
57.3	0.115	0.022	−0.415	0.051	*189.50*	*0.121*	*0.007*	*−0.148*	0.070
63.93	0.155	0.062	−0.284	0.013	194.15	0.107	0.001	0.414	0.016
78.98	0.205	0.031	0.391	0.001	198.18	0.137	0.006	0.504	0.035
85.50	0.157	0.048	0.754	0.058	199.05	0.176	0.006	0.204	0.022
88.5	0.130	0.044	0.938	0.068	199.50	0.146	0.048	0.231	0.079
98.01	0.170	0.021	1.048	0.046	201.39	0.155	0.025	0.042	0.037
104.00	0.156	0.014	1.098	0.028	206.15	0.129	0.002	0.138	0.027
115.64	0.158	0.022	1.097	0.030	206.57	0.229	0.085	0.232	0.095
125.80	0.142	0.035	1.098	0.064	209.46	0.100	0.006	0.839	0.013
126.04	0.145	0.008	1.084	0.011	212.08	−0.030	0.040	−0.082	0.112
128.40	0.125	0.064	1.145	0.007	215.40	0.125	0.035	0.181	0.118
136.2	0.101	0.012	0.853	0.003	217.89	0.131	0.008	0.472	0.412
141.4	0.118	0.006	0.649	0.011	219.79	0.089	0.004	0.681	0.023
144.00	0.101	0.001	0.589	0.016	220.00	0.072	0.010	0.661	0.007
150.89	0.070	0.011	0.483	0.040	220.85	0.141	0.061	0.789	0.026
155.40	0.127	0.006	0.730	0.026	221.44	0.113	0.028	0.929	0.045
161.95	0.138	0.005	0.744	0.001	222.11	0.113	0.002	0.751	0.007

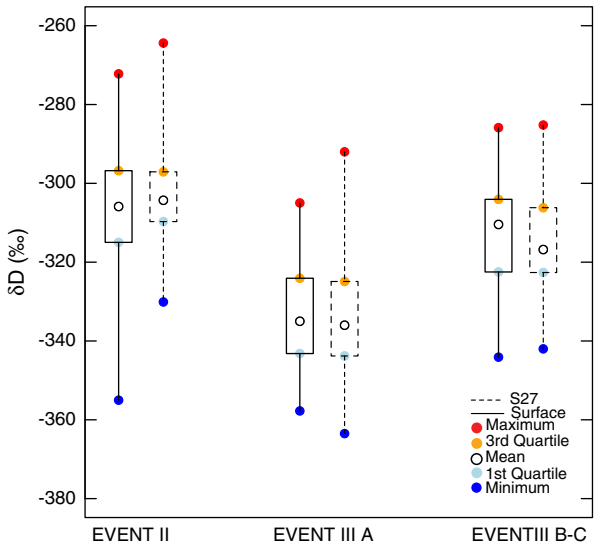

Figure 6. A boxplot comparison, using descriptive statistics of the shared events within δD measurements of surface ice and ice core S27, illustrates the similarity of the two records. There is a slight depletion trend in the δD of surface ice relative to that of ice core S27, which may be a result of snow accumulation at the end of transect A–B where ice flow is nearly stagnant. Overall their similarity indicates that the δD signature was not altered significantly when the ice became exposed at the surface.

variability over the upper 170 m and the full range of Pleistocene variability, from a minimum of −0.481‰ at 57.26 m to a maximum of +1.175‰ at 115.64 m. Below 170 m, scatter in the $\delta^{18}O_{atm}$ and $\delta^{15}N$ of N_2 data increases for reasons that are not yet clear, though internal mixing of the ice is one possibility. Measured $\delta^{15}N$ values of trapped N_2 average +0.125 ± 0.042‰, consistent with enrichment in ^{15}N due to gravitational fractionation in the diffusive zone of the firn at the site of accumulation. The magnitude of the gravitational enrichment in $\delta^{15}N$ is small compared to a number of other polar sites (e.g., ~+0.3 to +0.5‰ at Byrd, Vostok, and Dome C; Sowers et al., 1992), which we tentatively attribute to a thin diffusive zone (thick convective zone) in the firn at the site of accumulation.

Comparison of the environmental records developed from surface ice and S27

The similarities in the range of δD values observed in the surface ice and in ice core S27 are consistent with the hypothesis that the climate signal was not significantly altered when the ice became exposed at the surface. To compare the two δD profiles, they were placed on a common depth scale. The surface profile was correlated with the S27 ice core profile using sixteen tie-points. These tie-points include an ash layer observed at 3.76 m depth in S27 and 24.25 m downslope at the surface (Fig. 1). Surface distances between the tie-points were converted to S27 depths using linear interpolation.

When the δD records from ice core S27 and the surface ice are adjusted to the same time/depth scale and re-sampled to a minimum common resolution of 2.5 m, the initial observed similarity is confirmed. The two records have a Pearson correlation coefficient (r-value) of 0.81 ($p < 0.001$). A comparison of δD values for discrete intervals, corresponding to the Events shown in Figure 1, again indicates very little difference between the two records (Fig. 6). During Event II, S27 is 2.1‰ less negative, during Events IIIa and IIIb S27 is 0.3‰ more negative (less than the error of the measurement) and in Event IIIc S27 is 3‰ more negative. The slight trend of increasing enrichment in the surface samples, particularly those in Event IIIc, may be related to the decreased velocity at the northern end of the transect (nearest B). These samples were collected along a portion of the flowline where horizontal velocities are <10 cm yr^{-1} (Spaulding et al., 2012) and patches of snow accumulate on surfaces protected from wind by the surrounding ice ridges. We observed over two field seasons radical changes in snow cover throughout this part of the AH BIA. Similar observations are noted from satellite monitoring of blue ice patches near Byrd Glacier (Brown and Scambos, 2004). The higher measured δD values and increased variability in these samples could be related to isotopic diffusion between the recently accumulated snow (δD value of ~255‰) and the old ice at the surface via the mechanisms discussed by Rempel and Wettlaufer (2003). The impact of these possible diffusion processes was only observed for the portion of transect A–B where

Table 4
Surface to S27 distance/depth tie-points.

Distance from site 1 (km)	Depth of S27 (m)
0.86	224.23
0.94	220.99
1.00	216.80
1.10	211.39
1.17	203.00
1.19	195.00
1.38	183.62
1.49	164.05
1.59	166.00
1.84	112.24
1.88	108.38
2.06	85.09
2.19	76.50
2.31	63.85
2.42	41.98
2.50	23.49
2.65	3.76
2.67	0.00

Table 5
Tie-points for linear interpolation of AH integrated δD record to EDC3 timescale. Please note, the precision of the tie-point ages and depths does not indicate the uncertainty of the time scale created.

EDC3 (ka)	AH surface distance (km)	S27 depth (m)
86.700	5.196	–
89.668	4.996	–
93.278	4.506	–
98.533	3.936	–
103.492	3.666	–
108.395	2.950	–
114.361	–	1.545
116.168	–	12.555
121.902	–	39.289
124.189	–	47.241
126.508	–	58.548
128.206	–	74.908
128.634	–	84.930
128.967	–	87.860
136.147	–	128.320
156.044	–	158.690
158.293	–	161.325
159.105	–	163.305
161.210	–	165.065
162.476	–	166.615
164.198	–	170.355
175.842	–	174.930
179.182	–	177.055
187.732	–	182.950
190.400	–	184.595
192.026	–	185.500
193.264	–	186.985
203.500	–	198.845
221.400	–	206.650
224.331	–	208.265
244.828	–	216.225
245.330	–	218.680
249.000	–	221.335
253.000	–	223.075
254.500	–	224.225

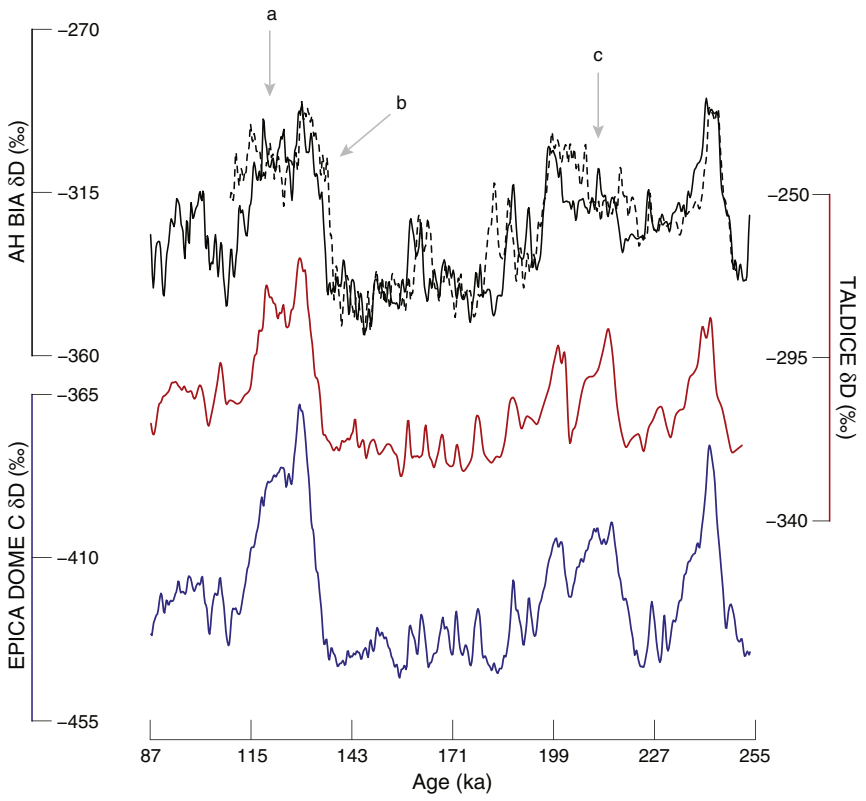

Figure 7. The AH integrated δD record is plotted on two separate timescales developed using comparison of AH BIA δD (solid black) and $\delta^{18}O_{atm}$ (dashed black) with the EDC and Vostok ice-core records (respectively). The δD records from EDC and TALDICE ($\delta^{18}O * 10$) are provided for comparison. All records are re-sampled (0.25 ka) and smoothed (5-point binomial filter). Arrows a, b, and c indicate sections where the AH integrated and TALDICE δD records show unique observable commonalities (a) and differences (b and c).

recently accumulated snow protects the surface ice from active sublimation during the austral summer season. The key point is that alteration of the δD in surface samples is either non-existent or very small.

The observed correlation is further supported by comparison of $\delta^{18}O_{atm}$ values at three of the shallow sites to measured $\delta^{18}O_{atm}$ values in the S27 core (Table 3). In general, the records of δD and $\delta^{18}O_{atm}$ at the surface and within S27 are in good agreement, suggesting that the horizontal/near-surface ice strata of the AH BIA contains the same stable water isotope and gas records as their vertical counterparts. By splicing the two records at their point of intersection we created a record with increased temporal coverage and resolution (Fig. 4c). Hereafter this spliced data set will be referred to as the "AH integrated δD record".

Table 6
Pearson correlation coefficients for the S27, AH Surface and AH integrated δD records and all other published ice core δD records fully covering the period 90–250 ka.

	AH surface	AH core (S27)	AH integrated	Epica Dome C	Vostok	Dome Fuji	Talos Dome
AH surface	1						
AH core (S27)	0.80	1					
AH integrated	–	–	1				
EPICA dome C	0.70	0.84	0.81	1			
Vostok	0.69	0.80	0.77	0.83	1		
Dome Fuji	0.64	0.74	0.70	0.76	0.92	1	
Talos Dome	0.72	0.80	0.76	0.92	0.77	0.69	1

Timescale development

Measurements of $^{40}Ar_{atm}$ from transect A–B and ice core S27 indicate that ice within the AH BIA is ~270 ± 300 ka. The range of δD values suggests that Event II corresponds to an especially warm interglacial period. Combined, these observations indicate that Event II of the AH integrated δD record could be ascribed to one of three time periods: the Holocene, Marine Oxygen Isotope Stage (MIS) 5.5, or MIS 9.3. In the following sections, the fit with each time period is assessed through comparison of δD trends with those in the EDC δD record (Fig. 4d). The

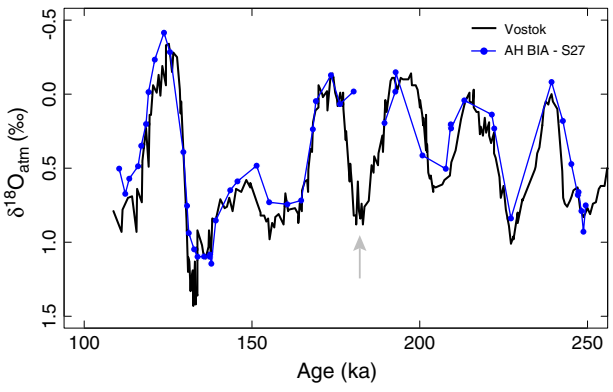

Figure 8. $\delta^{18}O_{atm}$ measurements from ice core S27 are compared with the same property from the Vostok ice core for the interval between 110 and 250 ka. The variability we observe in $\delta^{18}O_{atm}$ can be reasonably fit to the data from Vostok assuming one of the five maxima seen in Vostok is missing from S27 due to coarse sampling resolution and or internal deformation. The location of the missing maxima between ~175 and 190 ka is indicated by the gray arrow.

EDC δD record and EDC3 age scale (Jouzel et al., 2007; Parrenin et al., 2007) are chosen to determine a possible age match, as EDC exhibits minimal glaciological bias (Dreyfus et al., 2007) and the EDC3 age-scale has been mostly supported by absolute dating of tephra layers at Mt. Moulton (Popp et al., 2004; Dunbar et al., 2008) and by the newly developed AICC2012 (Bazin et al., 2012).

Within the AH BIA surface δD record, transitions both into and out of Event II are similar in magnitude to the transition into/out of maximum interglacial warmth. A decrease in δD/temperature of similar magnitude has not occurred since the transition to the Holocene making it the least favorable possible interpretation. MIS 9.3 can also be ruled out based on incompatibility with the δD record. Transitions into and out of Event II in the AH BIA surface δD record are similar to those of MIS 9.3, however Events I and III cannot be adequately matched, even when the higher resolution S27 δD record is considered. This is most obvious for event IIIc, which features a prominent double peak for which there is no peak of similar shape or magnitude prior to MIS 9.3 in the EDC record.

An approximate chronostratigraphy for the AH δD records was created by visually selecting similar features in both the EDC and AH integrated δD records (35 in total — Table 5), assigning EDC3 ages to selected AH depth/distances and linearly interpolating between them. This approach is based on observations of synchronous climate change on multi-millennial timescales as recorded in a number of deep ice cores drilled in East Antarctica (Watanabe et al., 2003; Stenni et al., 2011). Using these tie-points we find that the AH integrated δD record encompasses the time period from ~90 to 250 ka (Fig. 7).

After re-sampling the AH and EDC δD records to a common 250-yr resolution, and performing a statistical comparison, the AH surface, S27, and AH integrated δD records have Pearson correlation coefficients (r) of 0.70, 0.82, and 0.82 ($p < 0.001$) respectively, with the same interval in EDC record (Table 6). These numbers are similar to the r-values that can be calculated among each of the orbitally tuned timescales of the Antarctic deep core records available for this time period (Kawamura et al., 2007; Parrenin et al., 2007; Suwa and Bender, 2008; Stenni et al., 2011), which supports the assignment of Event II to the MIS 5.5 time interval.

A separately derived timescale based on $\delta^{18}O_{atm}$ from ice core S27 provides an additional means to evaluate the δD-based timescale. To create the $\delta^{18}O_{atm}$-based timescale, eight of the fifty $\delta^{18}O_{atm}$ measurements were assigned ages from the Suwa and Bender O_2/N_2 Vostok chronology (Suwa and Bender, 2008). As above, linear interpolation was used between the tie-points. When placed on this secondary timescale, the $\delta^{18}O_{atm}$ signal from S27 is similar to that seen in Vostok between ~110 and 250 ka (Fig. 8). The primary exception is that the record of $\delta^{18}O_{atm}$ from S27 contains only four maxima between 150 and 250 ka whereas the $\delta^{18}O_{atm}$ record from Vostok has five. One possibility is that the missing peak (between ~175 ka and 190 ka) has not been sampled, and we note that the maximum distance between consecutive samples in this interval is the largest within S27 at ~6 m. Alternatively, the record from S27 may not be continuous due to mixing or internal deformation, though this is not suggested by the higher-resolution δD measurements.

Placing the δD measurements from S27 on the $\delta^{18}O_{atm}$-based timescale validates the δD-based timescale as both suggest a temporal coverage of ~110–250 ka. For <90% of the measurements in S27, the assigned ages have a difference of ±4.5 ka between the two timescales. That difference is within the 6 ka uncertainty typically associated with $\delta^{18}O_{atm}$ constrained ice-core chronologies (Bender et al., 1994; Petit et al., 1999; Dreyfus et al., 2007). The gas age–ice age difference within S27 has yet to be established and we note that it could vary if changes in the snow accumulation source area (as discussed below) did occur. The $\delta^{18}O_{atm}$-based timescale thus assumes no gas age–ice age difference and this may contribute to some of the uncertainty in lining up the two chronologies. Given the overall agreement between the δD and $\delta^{18}O_{atm}$-based time scales for S27, we feel confident that the near-surface δD record (and thus the AH integrated δD record) covers the time period from ~90 to 250 ka, as suggested by the δD-based timescale.

Until additional analyses have been completed, including tephra-layer dating and measurement of CH_4 and CO_2 gases, the uncertainty in the timescales will preclude comparison of precisely timed events, however we believe our findings provide strong support for the value of a continued search for old ice in the AH BIA. For example, if we make a simplified calculation assuming that the linear age-depth trend of the last 50 m of S27 continues unchanged throughout the 100 m of ice not collected, the age of the ice nearest bedrock would be at minimum ~ 400 ka. A similar calculation using the age-distance trend of the 500 m prior to the final matched distance of the surface transect (860 m), yields minimum ages of ~400 ka for the ice at the end of the transect A–B as well. We also note that lenses of ice frozen to the bedrock, if found, could yield significantly older ages and that preliminary trapped gas measurements suggest this may be the case for the AH BIA location discussed in Harvey et al. (1998).

Ice dynamic impact on annual resolution

The developed δD-based chronostratigraphy indicates that 700 m of MIS 5.5 (116–132.6 ka) with a nominal resolution of 23.7 yr m^{-1} and 410 m of MIS 7 (186–245 ka) at 144.1 yr m^{-1} of ice are available at the AH BIA surface. These potential sampling resolutions are at least twice as detailed as those possible for any Antarctic deep-core record covering this time interval (Masson-Delmotte et al., 2011). The increased surface exposure and the consequent enhanced resolution result from the dipping and extension of the layers within the flowing ice. Given our original sampling resolution of 10 m, we cannot determine how these processes impacted the record on sub-millennial scales.

Within ice core S27, MIS 5.5 contains 96.7 m of ice with a resolution of 171.5 yr m^{-1}, while MIS 7 contains 35.5 m with a resolution of 880.5 yr m^{-1}. These resolutions are lower than those calculated for the Vostok, Dome Fuji and EDC ice cores. Accumulation rates at Allan Hills, like those of other coastal Antarctic ice cores (e.g. EDML, TALDICE and Taylor Dome) are 2–4 times higher than those for the plateau cores listed above (Arthern et al., 2006). Given the higher accumulation within the modern day "coastal" accumulation source of the AH BIA, the decreased annual layer thickness of S27 as compared to the Antarctic plateau cores suggests that considerable ice thinning has taken place. The thinning, which likely results from ice flow over dry bedrock, has similarly impacted the TALDICE and Taylor Dome ice cores. Nevertheless our data indicate that paleoclimate records from the AH BIA are of considerable value as they offer higher resolution and potentially longer temporal coverage than any other ice core recovered from the Ross Sea Sector of the continent. In addition within the BIA, cores covering selected time periods could be drilled in dry holes and dedicated entirely to measurements that require more ice than what would be available when fluid-filled holes are drilled for comprehensive ice-core studies.

Paleoclimatic interpretations

Both trapped gases and stable water isotopes along transect A–B confirm that the AH BIA has preserved a record of climate that is similar in its major features to existing paleoclimate records. Because the accumulation area for ice feeding into the AH BIA is very proximal, we anticipated that the AH BIA δD record would be most similar to that of the nearby Taylor Dome ice core (Steig et al., 2000). Given the low resolution of the Taylor Dome record for the overlapping time period, this comparison was difficult to make, thus we choose to compare the AH integrated δD record to the slightly more distal, but more highly resolved Talos Dome ice core (TALDICE — Masson-Delmotte et al., 2011; Stenni et al., 2011). We find that the two records are quite similar. This is most apparent for the latter portion of MIS 5.5 (Fig. 7, arrow "a")

in which both the AH integrated δD and TALDICE $\delta^{18}O$ records show a secondary warming of 1–3°C (using the 4‰/°C isotope-temperature relationship established at Taylor Dome for the AH BIA calculation; Steig et al., 1998). This warming is followed at both sites by an abrupt decrease in temperature at ~118 ka. The remaining records covering this time period (see Masson-Delmotte et al., 2011) either maintain temperature until 118 ka or begin to decrease immediately at ~126 ka.

There are also dissimilarities between the AH integrated and TALDICE δD records, which could be exploited to help clarify the climate history of the Ross Sea sector of Antarctica. One example is Termination II, which is recorded as a steady increase in δD to an interglacial maximum at TALDICE (and in all other records covering this time period), but is found in the AH BIA to contain a short (~0.9 ka) decrease in δD of 3‰ (Fig. 7, arrow "b"). The temporary decrease observed for δD values during Termination II may be related to changes in regional atmospheric circulation. A study by Scarchilli et al. (2010) suggests that during glacial maximum and deglacial periods the presence of an ice sheet in the Ross Sea reduces the transport of moisture sourced from the Pacific Ocean to the Transantarctic region. This reduction is compensated by an increase in the transport of moisture via a shorter, warmer distillation pathway from the Indian Ocean. The loss of some portion of the ice sheet and the ensuing switch to a more long-traveled source could explain the temporary reduction of δD values. Alternately, the observed reduction may result from an increase in the source elevation of ice flowing into the AH BIA. It has been suggested by previous researchers (Cassidy, 1983; Cassidy et al., 1992; Delisle, 1993; Coren et al., 2003) that ice may come from farther inland during ice-thickness high-stands related to increased precipitation at the inception of interglaciations. The increases in ice thickness associated with this process could have caused migration of the local ice divide just prior to the peak warmth of MIS 5.5. Doing so would have extended the accumulation area for the Allan Hills farther into the interior of the continent, causing an apparent disruption of the warming trend. Stratigraphic disturbance cannot be ruled out as a cause of the δD reversal discussed above, however no anomalies are seen within the $\delta^{18}O_{atm}$ samples encompassing that time period.

A second example occurs within MIS 7.3, where the observed δD values are much lower at the AH BIA than they are at nearby locations (Fig. 7, arrow "c"). Currently conflicting lines of evidence point to both MIS 5 and MIS 7 as potential candidates for the complete or partial collapse of the Ross and West Antarctic ice sheets (e.g. Stuiver et al., 1981; Bohaty et al., 1998; Kopp et al., 2009; McKay et al., 2012 for MIS 5 and Pollard and DeConto, 2009 for MIS 7). Further examination of this interval from within AH BIA proxy records could help to clarify the timing of the hypothesized collapse, as well as shed light on other aspects of this time period not captured in central East Antarctic ice cores.

Conclusions

Our data indicate that ice within the main icefield of the AH BIA is most likely stratigraphically continuous and contains a climate record that is in large part consistent with other published records. Comparison of δD measurements from ice collected at the surface along transect A–B with those from ice collected up to 225 m depth in ice core S27 suggest no significant alteration of the stable water isotope record when ice is exposed to the surface. Using $^{40}Ar_{atm}$ measurements from ice core S27 and a series of shallow cores along transect A–B, the age of the ice along the established flow line is constrained to 0–584 ka. Comparison of the δD and $\delta^{18}O_{atm}$ measurements from the AH BIA with those from published ice core records suggest the ice encompasses the time period from 90–250 ka. The sampled time period is intriguing as a multitude of records and modeling efforts suggest possible collapse of the Ross Ice Shelf and subsequently the WAIS during either MIS 5 or 7 (Kopp et al., 2009; Pollard and DeConto, 2009; Mckay et al., 2012). At present only a single ice archive from the Ross Sea sector of Antarctica covers any portion of this time period (Mt Moulton as discussed by Custer, 2006; Popp, 2008; Korotkikh et al., 2011).

Given the proximity of the AH BIA to the Ross Ice Shelf and the relative ease with large volumes of ice can be collected there, the 100 m of ice remaining above bedrock at S27 and the oldest sections of transect A–B are valuable targets for future, detailed paleoclimate investigations. This ice likely extends to at least 400 ka, and potentially to 1 Ma. This is particularly exciting as our findings indicate that gas records are well preserved along the flowline as well. If recovered the remaining ice in the AH BIA might therefore allow the first high-resolution, multi-proxy ice core based inferences of the behavior of the Ross Ice Shelf and possibly the WAIS during MIS 11, which is the best-known analog for the present interglaciation (Howard, 1997; Berger, 2002).

Supplementary data to this article can be found online at http://dx.doi.org/10.1016/j.yqres.2013.07.004.

Acknowledgments

Funding for this work was provided by NSF grants ANT-0838843 and EAR-1027960. The authors wish to thank RPSC and Kenn Borek Air Ltd., Kristin Schild, Melissa Rohde, Audrey Yau, Mike Waszkiewicz, Calum Hamilton, Daniel Lesser and Ashley Suitter for logistical, field, and laboratory assistance. The authors also wish to acknowledge two anonymous reviewers whose insightful comments contributed greatly to the quality of this manuscript.

References

Arthern, R.J., Winebrenner, D.P., Vaughan, D.G., 2006. Antarctic snow accumulation mapped using polarization of 4.3-cm wavelength microwave emission. Journal of Geophysical Research 111, D06107.

Bazin, L., Landais, A., Lemieux-Dudon, B., Toye Mahamadou Kele, H., Veres, D., Parrenin, F., Martinerie, P., Ritz, C., Capron, E., Lipenkov, V., Loutre, M.-F., Raynaud, D., Vinther, B., Svensson, A., Rasmussen, S.O., Severi, M., Blunier, T., Leuenberger, M., Fischer, H., Masson-Delmotte, V., Chappellaz, J., Wolff, E., 2012. An optimized multi-proxy, multi-site Antarctic ice and gas orbital chronology (AICC2012): 120–800 ka. Climate of the Past Discussions 8, 5963–6009.

Bender, M., Sowers, T., Labeyrie, L., 1994. The Dole effect and its variations during the last 130,000 years as measured in the Vostok ice core. Global Biogeochemical Cycles 8, 363–376.

Bender, M., Sowers, T., Lipenkov, V., 1995. On the concentrations of O2, N2, and Ar in trapped gases from ice cores. Journal of Geophysical Research: Atmospheres 100 (D9), 18651–18660.

Bender, M.L., Barnett, B., Dreyfus, G.B., Jouzel, J.G., Porcelli, D., 2008. The contemporary degassing rate of ^{40}Ar from the solid Earth. Proceedings of the National Academy of Sciences 105, 8232–8237.

Berger, A., 2002. Climate: an exceptionally long interglacial ahead? Science 297, 1287–1288.

Bintanja, R., 1999. On the glaciological, meteorological and climatological significance of Antarctic blue ice areas. Reviews of Geophysics 37 (3), 337–359.

Bohaty, S.M., Scherer, R.P., Harwood, D.M., 1998. Quaternary diatom biostratigraphy and palaeoenvironments of the CRP-1 drillcore, Ross Sea, Antarctica. Terra Antarctica 5, 431–453.

Brown, I.C., Scambos, T.A., 2004. Satellite monitoring of blue-ice extent near Byrd Glacier, Antarctica. Annals of Glaciology 39, 223–230.

Cassidy, W.A., 1983. The remarkably low surface density of meteorites at Allan Hills and implications in this for climate change. In: Oliver, R.L., James, P.R., Jago, J.B. (Eds.), Antarctic Earth Science. Cambridge University Press, Cambridge, pp. 623–625.

Cassidy, W.A., Olsen, E., Yanai, K., 1977. Antarctica: a deep-freeze storehouse for meteorites. Science 198, 727–731.

Cassidy, W., Harvey, R.P., Schutt, J., Delisle, G., Yanai, K., 1992. The meteorite collection sites of Antarctica. Meteoritics 27, 490–525.

Coren, F., Delisle, G., Sterzai, P., 2003. Ice dynamics of the Allan Hills meteorite concentration sites revealed by satellite aperture radar interferometry. Meteoritics and Planetary Science 38, 1319–1330.

Craig, H., 1961. Isotopic variation in meteoric waters. Science 133, 1702–1703.

Custer, S., 2006. Eemian Records of $^{18}O_{atm}$ and CH_4 Correlated to the Vostok EGT4 Timescale from the Moulton Blue Ice Field, West Antarctica. Senior Thesis in Geosciences Pennsylvania State University.

Dansgaard, W., Johnsen, S.J., Clausen, H.B., Gundestrup, N., 1973. Stable isotope glaciology. Meddelelser om Grønland 197, 1–53.

Dansgaard, W., Johnsen, S.J., Clausen, H.B., Dahl-Jensen, D., Gundestrup, N.S., Hammer, C.U., Hvidberg, C.S., Steffensen, J.P., Sveilbjornsdottir, A.E., Jouzel, J., Bond, G., 1993. Evidence for general instability of past climate from a 250-kyr ice-core record. Nature 364, 218–220.

Delisle, G., 1993. Global change, Antarctic meteorite traps and the East Antarctic Ice Sheet. Journal of Glaciology 39, 397–408.
Delisle, G., Sievers, J., 1991. Sub-ice topography and meteorite finds near the Allan Hills and the Near Western ice field, Victoria Land, Antarctica. Journal of Geophysical Research 96, 15577–15587.
Dixon, D.A., Mayewski, P.A., Goodwin, I.D., Marshall, G.J., Freeman, R., Maasch, K.A., Sneed, S.B., 2011. An ice core proxy for northerly air mass incursions into West Antarctica. International Journal of Climatology 32, 1455–1465.
Dreyfus, G.B., Parrenin, F., Lemieux-Dudon, B., Durand, G., Masson-Delmotte, V., Jouzel, J., Barnola, J.M., Panno, L., Spahni, R., Tisserand, A., Siegenthaler, U., Leuenberger, M., 2007. Anomalous flow below 2700 m in the EPICA Dome C ice core detected using ^{18}O of atmospheric oxygen measurements. Climate of the Past 3, 341–353.
Dunbar, N.W., Kyle, P.R., McIntoch, W.C., Esser, R.P., 1995. Allan Hills, Antarctica: a new source of glacial tephrochronological data. Antarctic Journal of the United States 30 (5), 76–78.
Dunbar, N.W., McIntosh, W.C., Esser, R.P., 2008. Physical setting and tephrochronology of the summit caldera ice record at Mount Moulton, West Antarctica. Geological Society of America Bulletin 120, 796–812.
E.P.I.C.A. Members, 2004. Eight glacial cycles from an Antarctic ice core. Nature 429, 623–628.
E.P.I.C.A. Members, 2006. One-to-one coupling of glacial climate variability in Greenland and Antarctica. Nature 444, 195–198.
Emerson, S., Quay, P.D., Stump, C., Wilbur, D., Schudlich, R., 1995. Chemical tracers of productivity and respiration in the subtropical Pacific Ocean. Journal of Geophysical Research 100, 15873–15887.
Faure, G., Buchanan, D., 1987. Glaciology of the East Antarctic ice sheet at the Allan Hills: a preliminary interpretation. Antarctic Journal of the United States 22 (5), 74–75.
Faure, G., Grootes, P.M., Buchanan, D., Hagen, E.H., 1992. Oxygen isotope study of the ice fields surrounding the Reckling Moraine on the East Antarctic Ice Sheet. Contributions to Antarctic Research Series 57, 15–26.
Grootes, P.M., Stuiver, M., White, J.W.C., Johnsen, S., Jouzel, J., 1993. Comparison of oxygen isotope records from the GISP2 and GRIP Greenland ice cores. Nature 366, 552–554.
Fudali, R.F., 1982. Gravity measurements across the Allan Hills main meteorite collecting area. Antarctic Journal of the United States 17 (5), 58–60.
Fudali, R.F., 1989. Gravity measurements across and between the meteorite-bearing icefields west-southwest of the Allan Hills. Antarctic Journal of the United States 24 (5), 48–50.
Grootes, P.M., Steig, E.J., Stuiver, M., Waddington, E.D., Morse, D.L., Nadeau, M.J., 2001. The Taylor dome Antarctic $\delta^{18}O$ record and globally synchronous changes in climate. Quaternary Research 56, 289–298.
Harvey, R.P., 2003. The origin and significance of Antarctic meteorites. Chemie der Erde-Geochemistry 63, 93–147.
Harvey, R.P., Dunbar, N.W., McIntosh, W.C., Esser, R.P., Nishiizumi, K., Taylor, S., Caffee, M.W., 1998. Meteoritic event recorded in Antarctic ice. Geology 26, 607–610.
Howard, W.R., 1997. Palaeoclimatology: a warm future in the past. Nature 388, 418–419.
Jouzel, J., Alley, R.B., Cuffey, K.M., Dansgaard, W., Grootes, P., Hoffman, G., Johnsen, S.J., Koster, R.D., Peel, D., Shuman, C.A., 1997. Validity of the temperature reconstruction from water isotopes in ice cores. Journal of Geophysical Research 102, 26471–26487.
Jouzel, J., Masson-Delmotte, V., Cattani, O., Dreyfus, G., Falourd, S., Hoffman, G., Minster, B., Nouet, J., Barnola, J.M., Chappellaz, J., Fischer, H., Gallet, J.C., Johnsen, S., Leuenberger, M., Loulergue, L., Luethi, D., Oerter, H., Parrenin, F., Raisbeck, G., Raynaud, D., Schilt, A., Schwander, J., Selmo, E., Souchez, R., Spahni, R., Stauffer, B., Steffensen, J.P., Stenni, B., Stocker, T.F., Tison, J.L., Werner, M., Wolff, E.W., 2007. Orbital and millennial Antarctic climate variability over the past 800,000 years. Science 317, 793–796.
Kawamura, K., Parrenin, F., Lisiecki, L.E., Uemura, R., Vimeux, F., Severinghaus, J.P., Hutterli, M.A., Nakazawa, T., Aoki, S., Jouzel, J., Raymo, M.E., Matsumoto, K., Nakata, H., Motoyama, H., Fujita, S., Goto-Azuma, K., Fujii, Y., Watanabe, O., 2007. Northern Hemisphere forcing of climatic cycles in Antarctica over the past 360,000 years. Nature 448, 912–916.
King, J.C., Turner, J., 1997. Antarctic Climatology and Meteorology. Cambridge University Press, Cambridge, U.K.
Kopp, R.E., Simons, F.J., Mitrovica, J.X., Maloof, A.C., Oppenheimer, M., 2009. Probabilistic assessment of sea level during the last interglacial stage. Nature 462, 863–867.
Korotkikh, E.V., Mayewski, P.A., Handley, M.J., Sneed, S.B., Introne, D.S., Kurbatov, A.V., Dunbar, N.W., McIntosh, W.C., 2011. The last interglacial as represented in the glaciochemical record from Mount Moulton Blue Ice Area, West Antarctica. Quaternary Science Reviews 30, 1940–1947.
Lisiecki, L., Raymo, M.E., 2005. A Pliocene–Pleistocene stack of 57 globally distributed benthic $\delta^{18}O$ records. Paleoceanography 20, PA1003.
Machida, T., Nakazawa, T., Narita, H., Fujii, Y., Aoki, S., Watanabe, O., 1996. Variations and the CO_2, CH_4 and N_2O concentrations and $\delta^{13}C$ of CO_2 in the glacial period deduced from an Antarctic ice core, South Yamato. Proceedings of the NIPR Symposium on Polar Meteorology and Glaciology, 10, pp. 55–65.
Masson-Delmotte, V., Buiron, D., Ekaykin, A., Frezzotti, M., Gallee, H., Jouzel, J., Krinner, G., Landais, A., Motoyama, H., Oerter, H., Pol, K., Pollard, D., Ritz, C., Schlosser, E., Sime, L.C., Sodemann, H., Stenni, B., Uemura, R., Vimeux, F., 2011. A comparison of the present and last interglacial periods in six Antarctic ice cores. Climate of the Past 7, 397–423.
Mayewski, P.A., Meeker, D., Whitlow, S., Twickler, M.S., Morrison, M.C., Bloomfiled, P., Bond, G.C., Alley, R.B., Gow, A.J., Meese, D.A., Grootes, P.M., Ram, M., Taylor, K.C., Wumkes, W., 1994. Changes in atmospheric circulation and ocean ice cover over the North Atlantic during the last 41,000 years. Science 263, 1747–1751.
Mckay, R., Naish, T., Powell, R., Barrett, P., Scherer, R., Talarico, F., Kyle, P., Monien, D., Kuhn, G., Jackolski, C., Williams, T., 2012. Pleistocene variability of Antarctic Ice Sheet extent in the Ross Embayment. Quaternary Science Reviews 34, 93–112.
Moore, J.C., Nishio, F., Fujita, S., Narita, H., Pasteur, E., Grinsted, A., Sinisalo, A., Maeno, N., 2006. Interpreting ancient ice in a shallow ice core from the South Yamato (Antarctica) blue ice area using flow modeling and compositional matching to deep ice cores. Journal of Geophysical Research 111, D16302.
Nagata, T., 1978. A possible mechanism of concentration of meteorites within the meteorite ice field in Antarctica. Proceedings of the Second Symposium on Yamota Meteorites. Memoirs of National Institute of Polar Research, 8, pp. 70–92.
Nakawo, M., Nagoshi, M., Mae, S., 1988. A stratigraphic record of an ice core from the Yamato meteorite ice field, Antarctica. Annals of Glaciology 10, 126–129.
Nishiizumi, K., 2006. Terrestrial age survey of Antarctic meteorites. Antarctic Meteorite Newsletter 29, 3–4.
Nishiizumi, K., Welten, K., 2008. Terrestrial age survey of Antarctic meteorites. Antarctic Meteorite Newsletter 31, 7–8.
Nishiizumi, K., Elmore, D., Kubik, P., 1989. Update on terrestrial ages of Antarctic meteorites. Earth and Planetary Science Letters 93, 299–313.
Parrenin, F., Barnola, J., Beer, J., Blunier, T., Castellano, E., Chappellaz, J., Dreyfus, G., Fischer, H., Fujita, S., Jouzel, J., Kawamura, K., Lemieux-Dudon, B., Loulergue, L., Masson-Delmotte, V., Narcisi, B., Petit, J.R., Raisbeck, G., Raynaud, D., Ruth, U., Schwander, J., Severi, M., Spahni, R., Steffensen, J.P., Sevensson, A., Udisti, R., Waelbroeck, C., Wolff, E.W., 2007. The EDC3 chronology for the EPICA Dome C ice core. Climate of the Past 3, 485–497.
Petit, J.R., Jouzel, J., Raynaud, D., Barkov, N.I., Barnola, J.M., Basile, I., Bender, M.L., Chappellaz, J., Davis, M., Delaygue, G., Masson-Delmotte, V., Kotlyakov, M., Legrand, M., Lipenkov, V.Y., Lorius, C., Pepin, L., Ritz, C., Saltzman, E.S., Stievenard, M., 1999. Climate and atmospheric history of the past 420,000 years from the Vostok ice core, Antarctica. Nature 399, 429–436.
Pollard, D., Deconto, R.M., 2009. Modelling West Antarctic ice sheet growth and collapse through the past five million years. Nature 458, 329–332.
Popp, T., 2008. The Speed and Timing of Climate Change: Detailed Stable Isotope Records from NorthGRIP, Greenland and Mt. Moulton, West Antarctica. (PhD Dissertation) Department of Geological Sciences, University of Colorado Boulder.
Popp, T.J., Sowers, T., Dunbar, N.W., McIntosh, W.C., White, J.W., 2004. Radioisotopically dated climate record spanning the last interglacial in ice from Mount Moulton, West Antarctica, Eos, Trans. AGU, Fall Meeting Abstract 84 (47), U31A–0015.
Raymo, M.E., Mitrovica, J.X., 2012. Collapse of polar ice sheets during the stage 11 interglacial. Nature 483, 453–456.
Rempel, A.W., Wettlaufer, J.S., 2003. Isotopic diffusion in polycrystalline ice. Journal of Glaciology 49, 397–406.
Scarchilli, C., Frezzotti, M., Ruti, P.M., 2010. Snow precipitation at four ice core sites in East Antarctica: provenance, seasonality and blocking factors. Climate Dynamics 37, 2107–2125.
Scherer, P., Schultz, L., Neupert, U., Knauer, M., Neumann, S., Leya, I., Michel, R., Mokos, J., Lipschutz, M., Metzler, K., Suter, M., Kubik, M., 1997. Allan Hills 88019: an Antarctic H-chondrite with a very long terrestrial age. Meteoritics and Planetary Science 32, 769–773.
Schultz, L., Annexstad, J.O., Delisle, G., 1990. Ice movement and mass balance at the Allan Hills Icefield. Antarctic Journal of the United States 25, 94–95.
Schwander, J., Stauffer, B., Sigg, S., 1988. Air mixing in firn and the age of the air at pore close-off. Annals of Glaciology 10, 141–145.
Severinghaus, J.P., Wolff, E.W., Brook, E.J., 2010. Searching for the oldest ice. Eos, Transactions of the American Geophysical Union 91, 357–358.
Shackelton, N.J., Opdyke, N.D., 1976. Oxygen isotope and paleomagnetic stratigraphy of Pacific core V28-239, late Pliocene to latest Pleistocene. In: Cline, R.M., Hays, J.D. (Eds.), Investigation of Late Paleoceanography and Paleoclimatalogy. Geological Society of America Memoirs, 145, pp. 449–464.
Sinclair, K.E., Bertler, N., Trompetter, W.J., 2010. Synoptic controls on precipitation pathways and snow delivery to high-accumulation ice core sites in the Ross Sea region, Antarctica. Journal of Geophysical Research 115, D22112.
Sinisalo, A., Grinsted, A., Moore, J.C., Meijer, H.A., Martma, T., van de Wal, R.S.W., 2007. Inferences from stable water isotopes on the Holocene evolution of Scharffenbergbotnen blue-ice area, East Antarctica. Journal of Glaciology 53, 427–434.
Sowers, T., Bender, M., Raynaud, D., Korotkevich, Y., 1992. The $\delta^{15}N$ of N_2 in air trapped in polar ice: A tracer of gas transport in the firn and a possible constraint on Ice age-Gas age differences. Journal of Geophysical Research 97, 15683–15697.
Spaulding, N.E., Spikes, V.B., Hamilton, G.S., Mayewski, P.A., Dunbar, N.W., Harvey, R.P., Schutt, J., Kurbatov, A.V., 2012. Ice motion and mass balance at the Allan Hills blue-ice area, Antarctica, with implications for paleoclimate reconstructions. Journal of Glaciology 58, 399–406.
Steig, E.J., Brook, E.J., White, J.C.W., Sucher, C.M., Bender, M.L., Lehman, S.J., Morse, D.L., Waddington, E.D., Clow, G.D., 1998. Synchronous climate changes in Antarctica and the North Atlantic. Science 282, 92–95.
Steig, E.J., Morse, D.L., Waddington, E.D., Stuiver, M., Grootes, P.M., Mayewski, P.A., Twickler, M.S., Whitlow, S.I., 2000. Wisconsinan and Holocene climate history from an ice core at Taylor Dome, western Ross Embayment, Antarctica. Geografiska Annaler: Series A, Physical Geography 82, 213–235.
Stenni, B., Buiron, D., Frezzotti, M., Barbante, C., Bard, E., Barnola, J.M., Baroni, M., Baumgartner, M., Capron, E., Castellano, E., Chappellaz, J., Delmonte, B., Falourd, S., Iacumin, P., Jouzel, J., Kipfstuhl, S., Landais, A., Lemieux-Dudon, B., Maggi, V., Masson-Delmotte, V., Mazzola, C., Minster, B., Montagnat, M., Mulvaney, R., Narcisi, B., Oerter, H., Parrenin, F., Petit, J.R., Ritz, C., Scarchilli, C., Schilt, A., Schu¨pbach, S., Schwander, J., Selmo, E., Severi, M., Stocker, F., Udisti, R., 2011. Expression of the bipolar see-saw in Antarctic climate records during the last deglaciation. Nature Geoscience 4, 46–49.

Stuiver, M., Denton, G.H., Hughes, T.J., Fastook, J., 1981. History of the marine ice sheet in West Antarctica during the last glaciation: a working hypothesis. In: Denton, G.H., Hughes, T.J. (Eds.), The Last Great Ice Sheets. John Wiley, New York, pp. 319–436.

Suwa, M., Bender, M.L., 2008. Chronology of the Vostok ice core constrained by O_2/N_2 ratios of occluded air, and its implication for the Vostok climate records. Quaternary Science Reviews 27, 1093–1106.

Tzedakis, P.C., Wolff, E.W., Skinner, L.C., Brovkin, V., Hodell, D.A., McManus, J.F., Raynaud, D., 2012. Can we predict the duration of an interglacial? Climate of the Past 8, 1473–1485.

Watanabe, O., Jouzel, J., Johnsen, S., Parrenin, F., Shoji, H., Yoshida, N., 2003. Homogeneous climate variability across East Antarctica over the past three glacial cycles. Nature 422, 509–512.

Whillans, I.M., Cassidy, W.A., 1983. Catch a falling star: meteorites and old ice. Science 222, 55–57.

Winograd, I.J., Coplen, T.B., Landwehr, J.M., Riggs, A.C., Ludwig, D.R., Szabo, J.B., Kolesar, P.T., Revesz, K.M., 1992. Continuous 500,000-year climate record from vein calcite in Devils Hole, Nevada. Science 258, 255–260.